Journal of Controlled Release 246 (2017) 98–109

Contents lists available at ScienceDirect

Journal of Controlled Release

journal homepage: www.elsevier.com/locate/jconrel

Gene Delivery

Blood-brain barrier-penetrating amphiphilic polymer nanoparticles deliver docetaxel for the treatment of brain metastases of triple negative breast cancer

Chunsheng He [a,1], Ping Cai [a,1], Jason Li [a,1], Tian Zhang [a], Lucy Lin [a], Azhar Z. Abbasi [a], Jeffrey T. Henderson [a], Andrew Michael Rauth [b], Xiao Yu Wu [a,*]

[a] Advanced Pharmaceutics and Drug Delivery Laboratory, Leslie Dan Faculty of Pharmacy, University of Toronto, Toronto, Ontario M5S 3M2, Canada
[b] Departments of Medical Biophysics and Radiation Oncology, Faculty of Medicine, University of Toronto, Toronto, Ontario M5G 2M9, Canada

ARTICLE INFO

Article history:
Received 10 November 2016
Accepted 19 December 2016
Available online 23 December 2016

Keywords:
Blood-brain barrier
Amphiphilic polymer nanoparticles
Brain metastases
Triple-negative breast cancer
Docetaxel delivery
Chemotherapy

ABSTRACT

Brain metastasis is a fatal disease with limited treatment options and very short survival. Although systemic chemotherapy has some effect on peripheral metastases of breast cancer, it is ineffective in treating brain metastasis due largely to the blood-brain barrier (BBB). Here we developed a BBB-penetrating amphiphilic polymer-lipid nanoparticle (NP) system that efficiently delivered anti-mitotic drug docetaxel (DTX) for the treatment of brain metastasis of triple negative breast cancer (TNBC). We evaluated the biodistribution, brain accumulation, pharmacokinetics and efficacy of DTX-NP in a mouse model of brain metastasis of TNBC. Confocal fluorescence microscopy revealed extravasation of dye-loaded NPs from intact brain microvessels in healthy mice. DTX-NP also extravasated from brain microvessels and accumulated in micrometastasis lesions in the brain. Intravenously injected DTX-NPs increased the blood circulation time of DTX by 5.5-fold and the $AUC_{0-24\ h}$ in tumor-bearing brain by 5-fold compared to the clinically used DTX formulation Taxotere®. The kinetics of NPs in the brain, determined by *ex vivo* fluorescence imaging, showed synchronization with DTX kinetics in the brain measured by LC-MS/MS. This result confirmed successful delivery of DTX by the NPs into the brain and suggested that *ex vivo* fluorescence imaging of NP could be an effective and quick means for probing drug disposition in the brain. Treatment with the DTX-NP formulation delayed tumor growth by 11-fold and prolonged median survival of tumor-bearing mice by 94% compared to an equivalent dose of Taxotere®, without inducing histological changes in the major organs.

© 2016 Elsevier B.V. All rights reserved.

1. Introduction

Brain metastasis of breast cancer (BMBC) occurs in an estimated 15–30% of breast cancer patients [1–4]. Patients with triple-negative breast cancer (TNBC) or human epidermal growth factor receptor 2 (HER-2) positive breast cancer are at higher risk of developing BMBC compared to patients with other breast cancer subtypes [1–5]. The prognosis of patients with TNBC is particularly poor due to the lack of effective therapies against TNBC and its aggressive biology [6]. While chemotherapy is routinely used to control peripheral metastasis of breast cancer, it is largely ineffective at treating metastatic lesions in the brain due to poor drug penetration through the blood brain barrier (BBB). The BBB is composed of a collection of endothelial and neuronal cells which operate as a physical, enzymatic and transport barrier at the brain-blood interface to regulate entry of molecules into the central nervous system [7,8]. It is estimated that about 98% of central nervous system (CNS) drugs fail to enter clinical trials due to poor brain penetration [9]. While the brain tumor-associated BBB is structurally impaired and more permeable compared to the healthy BBB, it still represents a significant barrier to drug delivery to brain metastases [10].

Various invasive approaches have been investigated to enhance drug delivery to the brain by cannula-mediated drug delivery (*i.e.* intrathecal, intraventricular, or intratumoral injection, and convection-enhanced delivery) or BBB-disruption using hyperosmotic solutions and vasoactive compounds [11]. The applicability of these methods are limited due to non-specific influx of drug molecules and fluid into CNS which can potentially lead to neurological toxicity, aphasia and hemiparesis [12]. Systemic strategies for the treatment of BMBC include identification of novel BBB-permeable drugs suitable for prevention or treatment of BMBC [13–19], or delivery of clinically established BBB-impermeable chemotherapy drugs across the BBB by conjugation to ligands which bind specific receptors found on the brain endothelial cells, including the transferrin receptor [8,20–22], low density lipoprotein (LDL) receptor [23,24], insulin receptor [25], or glutathione

* Corresponding author.
E-mail address: xywu@phm.utoronto.ca (X.Y. Wu).
[1] These authors contributed equally to this work.

http://dx.doi.org/10.1016/j.jconrel.2016.12.019
0168-3659/© 2016 Elsevier B.V. All rights reserved.

receptor [26]. Binding of the antibody-drug conjugates to their respective receptors enables receptor-mediated transcytosis of the drug across the BBB.

In the past decade, drug-loaded nanocarrier systems with surface conjugated ligands that target the same receptors have also been explored [27–29]. The nanocarrier systems show advantages over drug-ligand conjugates including their high drug loading capacity, prolonged blood circulation time, sustained drug release, and reduction of enzyme-mediated drug degradation [8,30]. It has been found that nanoparticles (NP) coated with polysorbate 80 (PS 80), after adsorption of apolipoproteins in the blood circulation, may mimic LDL particles facilitating the entry of NP to the brain *via* LDL receptor-mediated transcytosis [23,31]. A number of published works have demonstrated the effectiveness of PS 80-coated NP in the delivery of chemotherapy drugs across the BBB for the treatment of glioblastoma multiforme [24,32–35]. We previously developed a PS 80-containing biocompatible polymer system based on poly(methacrylic acid) and maltodextrin [36,37], and demonstrated its ability to deliver ionic drug, such as doxorubicin, across the BBB in healthy mice and brain metastasis [30]. Given the low cost of PS 80 and its approved use in many injectable pharmaceutical products, PS 80-modified polymer system offers tremendous potential compared to other BBB-targeting ligands.

In this study, a novel PS 80-based amphiphilic polymer nanocarrier system was developed to encapsulate DTX by self-assembly for the treatment of brain metastases of TNBC. DTX is a widely used anti-mitotic drug for the treatment of locally advanced and metastatic breast cancers [38–41], and for the treatment of extracranial TNBC [42]. However, DTX has not been applied to treat brain metastases as it is subject to P-gp efflux at the BBB and is unable to accumulate in the brain at adequate levels [43,44]. Furthermore DTX is practically insoluble in water and thus the clinically used product of DTX, Taxotere® is formulated as an alcohol-water mixture with high PS 80 content that is believed to cause hypersensitivity in some patients [45]. Recently a number of NP formulations of DTX have been developed and shown to increase DTX accumulation and efficacy in glioma xenografts in mice [46–48]. Nevertheless, no attempt to design DTX NP for treatment of brain metastases of TNBC has been reported, to the best of our knowledge.

To efficiently load and release the poorly water-soluble drug DTX, while maintaining the capability of the nanocarrier crossing the BBB, we have designed and optimized an amphiphilic polymer nanocarrier system for DTX and evaluated its biodistribution, brain accumulation, pharmacokinetics and preclinical efficacy in a murine brain metastasis model of human TNBC. The present work demonstrates that DTX-loaded NP is able to extravasate from brain microvessels and deliver DTX to brain metastases of TNBC following intravenous administration. The pharmacokinetics of DTX delivered by the NP in the brain was found to synchronize with the kinetics of fluorescence intensity of the NP in the *ex vivo* brain tissue suggesting that DTX entry into the brain was likely facilitated by NP transport across the BBB and that *ex vivo* imaging of NP fluorescence is a good indicator of drug disposition in the brain. Treatment with DTX-NP resulted in significantly extended DTX circulation, markedly higher DTX accumulation in the brain, and prolonged median survival time of brain tumor-bearing mice as compared to Taxotere®.

2. Materials and methods

2.1. Materials

Maltodextrin (Dextrose Equivalent = 16.5–19.5), methacrylic acid (MAA), sodium thiosulfate (STS), potassium persulfate (KPS), polysorbate 80 (PS 80), sodium dodecyl sulphate (SDS), fluoresceinamine isomer I (FA), *N*-(3-dimethylaminopropyl)-*N*′-ethylcarbodiimide hydrochloride (EDC), *N*-hydroxysuccinimide (NHS), dodecylamine, ethyl arachidate, and all other chemicals unless otherwise mentioned were purchased from Sigma-Aldrich Canada (Oakville, ON, Canada). HiLyte Fluor ™ 750 hydrazide (HF 750) was purchased from AnaSpec (Fremont, CA, USA). Texas red-labeled dextran (MW 70,000 Da) was obtained from Life Technologies (CA, USA). DTX was purchased from LC Laboratories (Woburn, MA, USA). Taxotere® was purchased from Hospira Healthcare Corporation (Saint-Laurent, Québec, Canada). MDA-MB-231-luc-D3H2LN cell line was obtained from Caliper Life Sciences (Hopkinton, MA, USA) and was confirmed to be pathogen free by the supplier using IMPACT Profile I (PCR). These cells were passaged for <6 months following resuscitation.

2.2. Synthesis of amphiphilic polymer

The amphiphilic polymer was synthesized by covalently linking dodecylamine to the terpolymer (Supporting information, Scheme S1) of poly(methacrylic acid), polysorbate 80 and starch which was prepared using a method described previously [30]. Purified terpolymer (500 mg), EDC (80 mg), and NHS (80 mg) were dissolved in 5 mL of distilled de-ionized water (DDIW) and allowed to react for 1 h at room temperature. Between 0.1 and 1 mL of dodecylamine solution (40 mg/mL in dimethyl sulfoxide (DMSO)) was added to the activated terpolymer solution and allowed to react at 37 °C for 24 h. The final product solution was neutralized to pH 7.4 using 0.1 N NaOH, and purified by extensive dialysis (molecular weight cut-off (MWCO) = 12 kDa) against DMSO for 24 h and DDIW for 48 h at room temperature. The polymer solution was then lyophilized and stored in a desiccator at 4 °C. The molecular weight of the amphiphilic polymer was measured using static light scattering [49].

2.3. Synthesis of fluorescence dye-conjugated amphiphilic polymer

For *in vivo* and *ex vivo* imaging, two fluorescent dyes, namely HiLyte Fluor™ 750 (HF 750; λ_{ex} = 745 nm, λ_{em} = 820 nm) and FA (λ_{ex} = 496 nm, λ_{em} = 520 nm) were conjugated to the amphiphilic polymer using the following method: 500 mg of purified amphiphilic polymer was dissolved in 2 mL of aqueous solution containing 50 mg of EDC and 50 mg of NHS and stirred for 30 min at room temperature, followed by addition of 0.8 mg of HF 750 (1.25 mg/mL in DDI water (DDIW)) or 1.25 mg of FA (5 mg/mL in DMSO). The mixture was protected from light and stirred at room temperature for 24 h. Finally, the product was neutralized to pH 7.5 using 0.1 N NaOH and purified by extensive dialysis (MWCO = 12 kDa) against DDI water for 48 h. The dried dye conjugated-amphiphilic polymer was obtained by lyophilization and stored in a desiccator for future use.

2.4. Preparation of DTX-loaded amphiphilic polymer nanoparticles

To find optimal composition to achieve high DTX loading and good NP properties, amphiphilic polymer with varying amounts of dodecyl contents were used (Table 1). In a typical experiment, 12 mg of ethyl arachidate was added to a 15 mL conical tube, with or without addition of Nile Red (20 μL of 5 mg/mL stock in $CHCl_3$), and heated to 80 °C. Fifty microliters of 100 g/L Pluronic® F-68 (PF68) solution, DTX (200 μL of 10 mg/mL DTX in $CHCl_3$) and amphiphilic polymer (200 μL of 50 mg/mL in DDIW) were added to the solution and stirred for 20 min. The mixture was sonicated for 10 min using a Hielscher UP 100H probe ultrasonicator (Ringwood, NJ, USA) at 80% peak. Following sonication, the entire emulsion was quickly transferred into 1 mL of saline (0.9% w/v NaCl) being stirred on ice. The particle size and zeta potential of the DTX-NP were measured with Malvern Zetasizer Nano ZS (Worcestershire, UK). For transmission electron microscopy (TEM), NP dispersed in DDI water were dried onto a carbon coated grid. The TEM images were acquired on a Hitachi H7000 electron microscope (Hitachi Canada, Ltd., Mississauga, Ontario, Canada) with an accelerating voltage of 100 kV.

Table 1
Compositions of amphiphilic polymer and their effect on the drug loading efficiency and content, and particle properties of docetaxel-loaded nanoparticle formulations.

Amphiphilicpolymer[a] (mg/mL)	Dodecyl[b] (%)	Ethyl Arachidate (mg/mL)	PF 68 (mg/mL)	Docetaxel (mg/mL)	Size (nm)	Polydispersity Index (PDI)	Zeta potential (mV)	Encapsulation efficiency (%)	Loading Content (%)
10	0	12	5	2	165.1 ± 3.2	0.36 ± 0.04	−51.1 ± 1.5	75.5 ± 2.5	5.3 ± 1.1
10	1	12	5	2	133.3 ± 4.3	0.26 ± 0.02	−49.1 ± 2.4	82.2 ± 1.8	5.74 ± 0.9
10	2	12	5	2	125.1 ± 5.4	0.21 ± 0.05	−50.1 ± 1.7	87.5 ± 2.4	6.09 ± 1.3
10	5	12	5	2	105.1 ± 1.5	0.19 ± 0.06	−49.1 ± 2.8	93.3 ± 1.6	6.46 ± 0.4
10	10	12	5	2	100.1 ± 2.6	0.17 ± 0.02	−48.1 ± 2.4	98.2 ± 1.0	6.78 ± 1.4

Add data presented as mean ± SD for n = 3 independent experiments.
[a] The molecular weight of the amphiphilic polymer was measured using static light scattering.
[b] The content of dodecylamine grafted onto amphiphilic polymer was calculated by molecular weight.

2.5. Determination of drug loading, encapsulation efficiency, stability and drug release kinetics

Immediately after formulation, DTX-NP suspension was diluted 4 times by PBS (pH = 7.45, containing 0.5% SDS), transferred to a centrifugal filter (MWCO = 30 kDa), and centrifuged for 15 min at a RCF of 21,100 × *g*. The free drug concentration in the filtrate was assayed at 232 nm using an ultraviolet-visible (UV–Vis) spectrometer (Agilent 8453). The drug loading (% wt drug/wt lipid) and encapsulation efficiency (% wt drug/wt total drug) were then calculated.

To determine the stability of the DTX-NP, 200 μL of NP were incubated in 2 mL of pH 7.4 PBS buffer, or 100% FBS at 37 °C for up to 72 h. Aliquots were taken at different time intervals and diluted with DDIW for analysis of particle size and zeta potential (Malvern Zetasizer Nano ZS, Worcestershire, UK).

To determine *in vitro* drug release kinetics, DTX-NP suspension (1 mL) or free DTX solution with the same drug concentration (1 mL) was enclosed in a 14 kDa MWCO dialysis tube and immersed in 200 mL, pH 7.45 PBS (containing 0.5% SDS) at 37 °C with continuous magnetic stirring. At selected time intervals, 1 mL of aqueous solution was withdrawn from the release medium and the drug concentration was measured with spectrophotometry. The sample was placed back into the release system after measurement. Each release experiment was repeated 3 times and the mean and standard deviations of triplicates are reported.

2.6. In vitro cell uptake of nanoparticle

To evaluate the cell uptake of NR-DTX-NP, MDA-MB-231 cells were seeded at a density of 30,000 cells per well in 24-well plates and incubated for 24 h at 37 °C under 5% CO_2. Following the incubation, the medium was replaced with fresh medium (1 mL) and 20 μL of Nile red loaded DTX-NP (NR-DTX-NP) were added and incubated at 37 °C. At various incubation times, the NP-containing medium was removed and the cells were washed 3 times with cell culture medium. Cell nuclei were stained with Hoechst 33342 (Molecular Probes, Inc. Eugene. OR, USA). The cells were imaged on an AMG EVOSf1 fluorescence microscope (Invitrogen, Carlsbad, CA, USA) and Zeiss LSM700 confocal microscope with the filters for Nile red: Ex./Em. = 530/593 nm, and for Hoechst 33,342: Ex./Em. = 360/447 nm. The fluorescence intensity was measured using a microplate fluorescence reader (λ_{ex} = 530 nm, λ_{em} = 630 nm) to quantify the cellular uptake of the NPs.

2.7. In vitro cytotoxicity in triple negative human breast cancer cells

Cytotoxicity of Blank-NP (no DTX), DTX-NP and free DTX, were evaluated in triple negative human breast cancer cells MDA-MB-231-luc cells. The cells were seeded at a density of 7000 cells per well in 96-well plates and incubated for 24 h at 37 °C under 5% CO_2. Then the cells were treated for 24 h with various formulations at different concentrations. Cell viability was measured using the 3-(4,5-dimethylthiazol-2-yl)-2,5-diphenyltetrazolium bromide (MTT) assay and is expressed as the percent of control for each treatment group [50]. Cells with no treatment and cells incubated with Blank-NP were used as controls for the free drug and DTX-NP, respectively.

2.8. Animal model

All animal handling and procedures were conducted under an approved protocol from the Animal Care Committee at the Ontario Cancer Institute. An animal model for BMBC was established by injecting luciferase expressing human breast cancer cells (MDA-MB-231-luc-D3H2LN) (5×10^4 cells/mouse) intracranially into the cortex of four to six week old, severe combined immune deficiency (SCID) mice (Ontario Cancer Institute, Toronto, ON, Canada) using a stereotaxic system (SAS-5100, ASI Instruments, Warren, MI, USA) [30]. Tumor growth was monitored by luciferin-induced bioluminescence imaging (15 mg/kg luciferin, intraperitoneal injection 10 min prior to imaging) using a Xenogen IVIS spectrum imager (Caliper Life Sciences, Hopkinton, MA, USA). Formation of numerous micro-metastases in the cortical and subcortical regions was confirmed by H&E staining of brain tissue sections (Supporting information, Fig. S1).

2.9. Live animal and ex vivo optical imaging

Near-infrared (NIR) dye HiLyte Fluor ™ 750 (HF 750)- and Fluoresceinamine isomer I (FA)-labeled DTX-NP (200 μL injection volume; 10 mg/mL HF 750- and FA-amphiphilic polymer, 6.7 ± 0.1 μmol of HF 750 and 120 ± 0.2 μmol of FA per gram of polymer; 20 mg/kg DTX for tumor-bearing mice) were injected into the lateral tail vein of tumor-bearing mice. At pre-determined time points fluorescence images of the whole body and dissected organs (brain, heart, liver, and spleen) were obtained using the Xenogen IVIS spectrum imager (745 nm excitation, and 820 nm emission wavelengths). NP accumulation within the organs was reported as the ratio of NIR fluorescence intensity of NP-treated tissue to saline-treated tissue.

2.10. Confocal fluorescence microscopy for microdistribution of nanoparticles in brain tissue

2.10.1. Delivery of BBB-impermeable dye into healthy brain

Hoechst 33342-loaded FA-labeled amphiphilic polymer NP were prepared by a suspension-ultrasonication method. A mixture of 250 μL of Hoechst 33,342 solution (10 mg/mL), 200 μL of FA-amphiphilic polymer solution (50 mg/mL), 50 μL of PF 68 solution (100 mg/mL), and

12 mg of ethyl arachidate was heated to 80 °C and stirred for 20 min. NP were formed under ultrasonication using a Hielscher UP100H probe ultrasonicator, (Hielscher USA, Inc., Ringwood JN, USA) for 10 min and suspended in sterile 5% dextrose to a final Hoechst 33342 concentration of 2.5 mg/mL. An analogous control formulation was prepared from FA-amphiphilic polymer without PS 80. To examine NP penetration into healthy brain, SCID mice were treated with 200 μL of Hoechst 33,342-loaded NP with or without PS 80 (2.5 mg/mL dye), or free Hoechst 33342 (2.5 mg/mL in saline) *via* tail vein injection. Mice were euthanized 2 h following treatment. Texas red-labeled dextran (100 μL volume, 1% wt solution) was administered intravenously 15 min prior to euthanasia. The brain was dissected, fixed in 10% formalin for 3 h, transferred to 30% dextrose solution overnight, embedded in Tissue-Tek OCT resin (Somagen, Torrance, CA, USA) and finally flash frozen. Thaw mounted 20 μm thick frozen sections were prepared using a Leica CM3050S cryostat (Leica, Wetzlar, Germany) and analyzed using Zeiss LSM700 confocal microscope (Carl Zeiss, Jena, Germany) using fluorescent excitation and emission filters appropriate for detection of the indicated chromophores (Dextran, Texas Red: Ex./Em. = 595/615 nm; FITC: Ex./Em. = 490/520 nm; Hoechst 33342: Ex./Em. = 352/461 nm).

2.10.2. Nanoparticle microdistribution in tumor-bearing brain tissue

FA-labeled DTX-NP (200 μL injection volume; 10 mg/mL FA-amphiphilic polymer, 120 ± 0.2 μmol of FA per gram of polymer; 20 mg/kg DTX for tumor-bearing mice) were injected into the tail vein of tumor-bearing SCID mice. Two hours later Texas red-labeled dextran (100 μL volume, 1% wt. solution) was administered intravenously 15 min prior to euthanasia to label functional brain blood vessels [31]. The brains were processed and examined as described above. NP distribution around the tumor was examined within the FITC emission laser (Ex/Em. = 490/520 nm). Brain blood vessels were imaged over the Texas red spectral wavelengths (Ex./Em. = 595/615 nm). Cell nuclei were imaged within the DAPI spectral laser (Ex./Em. = 352/461 nm) after nuclear staining with Hoechst 33342 trihydrochloride, trihydrate (Invitrogen, 1:10,000 dilution) and 3× wash with pH 7.4 PBS.

2.11. Pharmacokinetic study of DTX-NP in brain tumor-bearing mice

Tumor-bearing mice were randomly allocated into two treatment groups and received a single i.v. injection of DTX-NP or Taxotere® at a matched dose of 20 mg DTX/kg. At 0.25, 0.5, 1, 2, 6 and 24 h after injection, whole blood was collected in heparinized tubes from ketamine anesthetized mice by cardiac puncture. Following perfusion with ice-cold saline *via* the left ventricle, the tumor-bearing brains were harvested, rinsed in PBS, weighted, snap-frozen and stored at −80 °C for further analysis. DTX was extracted from the mouse tissues by protein precipitation [51,52]. Tissue homogenate was prepared by adding 9 parts DDI water to 1 part whole blood or 3 parts DDI water to 1 part brain before homogenizing at 3600 rpm for 5 min using a Precellys 24 homogenizer (VWR, Erlangen, Germany). Tissue homogenate (36 μL) was added to 1.5 mL micro-centrifuge tubes, followed by the addition of 10 μL of methanol and 3.75 μL of 250 ng/mL paclitaxel solution as an internal standard. The mixture was vortexed for 1 min. Methanol/acetonitrile mixture (100.25 μL, 1:1 (v/v)) was then added to the tubes and vortexed for 10 min to precipitate the protein. The samples were centrifuged for 15 min at 21,100 × *g* and the supernatant was transferred to high performance liquid chromatography (HPLC) vials for analysis using liquid chromatography-dual mass spectroscopy (LC-MS/MS) (AB Sciex QStarXL Q-TOF mass spectrometer (AB Sciex, ON, Canada)). DTX transitions were detected by an AB Sciex API4000 triple quadrupole mass spectrometer equipped with an electrospray ionization interface (Advanced Instrumentation for Molecular Structure, Department of Chemistry, University of Toronto). The system was operated in positive ion mode. The multiple reaction monitoring (MRM) transitions monitored for DTX were *m/z* 544.0/361.1. Results are presented as drug mass per mass of tissue (ng DTX/mg tissue). Detailed protocols for modeling DTX disposition in mouse by a semi-physiologically-based pharmacokinetic (semi-PBPK) model are described in the Supporting information material.

2.12. Evaluation of therapeutic efficacy

To brain tumor-bearing SCID mice, DTX-NPs (20 mg DTX/kg, 200 μL administered i.v.), or an equivalent dose of Taxotere®, or saline (200 μL), or Blank-NP (equivalent NP mass to DTX loaded NP) were administered on day 0, typically between one to two weeks following tumor inoculation depending on desired initial tumor size. A second identical treatment was administered two weeks later on day 14. This dosing regimen was determined from dose tolerance studies (data not shown). Tumor growth was monitored *in vivo* using bioluminescence imaging for up to four weeks following the first treatment. The fold increase in total tumor size was obtained by normalizing the tumor radiance (TR) over the course of the experiment to the initial tumor radiance at day 0. Tumor growth delay (TGD) was calculated from the mean survival time of each group according to $TGD(\%) = \left(\frac{TR_{treated} - TR_{control}}{TR_{control}}\right) \times 100$ as previously reported [53].

Once the mice exhibited signs of discomfort (*i.e.* weight loss 20% off, lack of grooming, signs of self-mutilation, resistance to ambulation), defined as endpoint, mice were euthanized by cervical dislocation under 1% isofluorane anesthesia. Immediately after euthanasia, intact hearts, livers, lungs and kidneys were fixed in 10% neutral-buffered formalin, paraffin-embedded and stained with hematoxylin and eosin (H&E) for morphological evaluation, which was conducted by a board-certified veterinary anatomic pathologist.

2.13. Statistical data analysis

All data are presented as means ± standard deviation (SD). Student's *t*-test or analysis of variance (ANOVA) followed by Tukey *t*-test (OriginPro8) were utilized to determine statistical significance between two or more groups, respectively. p-Values < 0.05 were considered statistically significant.

3. Results and discussion

3.1. Design, synthesis and optimization of DTX-loaded amphiphilic polymer NP

In the present work we developed an amphiphilic polymer-lipid nanocarrier system for delivery of hydrophobic drug DTX to brain metastases of human breast cancer in a mouse model. The nanocarrier is comprised of solid lipid domain of ethyl arachidate stabilized with an amphiphilic copolymer comprised of a maltodextrin, poly(methacrylic acid) (PMAA), PS 80 and n-dodecane (Fig. 1a, Supporting information Scheme S1). Maltodextrin serves as the polymer backbone onto which PMAA is grafted to provide abundant carboxylic acid functional groups for further chemical modification with PS 80, dodecylamine and fluorescence probes. PS 80 has been previously reported to facilitate NP transport across the BBB [23,30,33,54]. Dodecyl groups render the polymer amphiphilic to facilitate affinity with the lipid domain. DTX was efficiently loaded into the NP through hydrophobic interaction with the dodecyl groups in the amphiphilic polymer and partitioning into the solid lipid domain. All materials used for NP synthesis are biocompatible/biodegradable and generally regarded as safe (GRAS) for injection.

To design an amphiphilic polymer NP carrier with optimal properties for efficient loading and release of DTX, the composition of amphiphilic polymer was optimized with varying dodecyl substitution content. The physicochemical properties of DTX-loaded NP (DTX-NP), including particle size, polydispersity, DTX encapsulation efficiency and DTX loading content, were characterized and summarized in Table 1 as a function of dodecyl content. NP with greater dodecyl

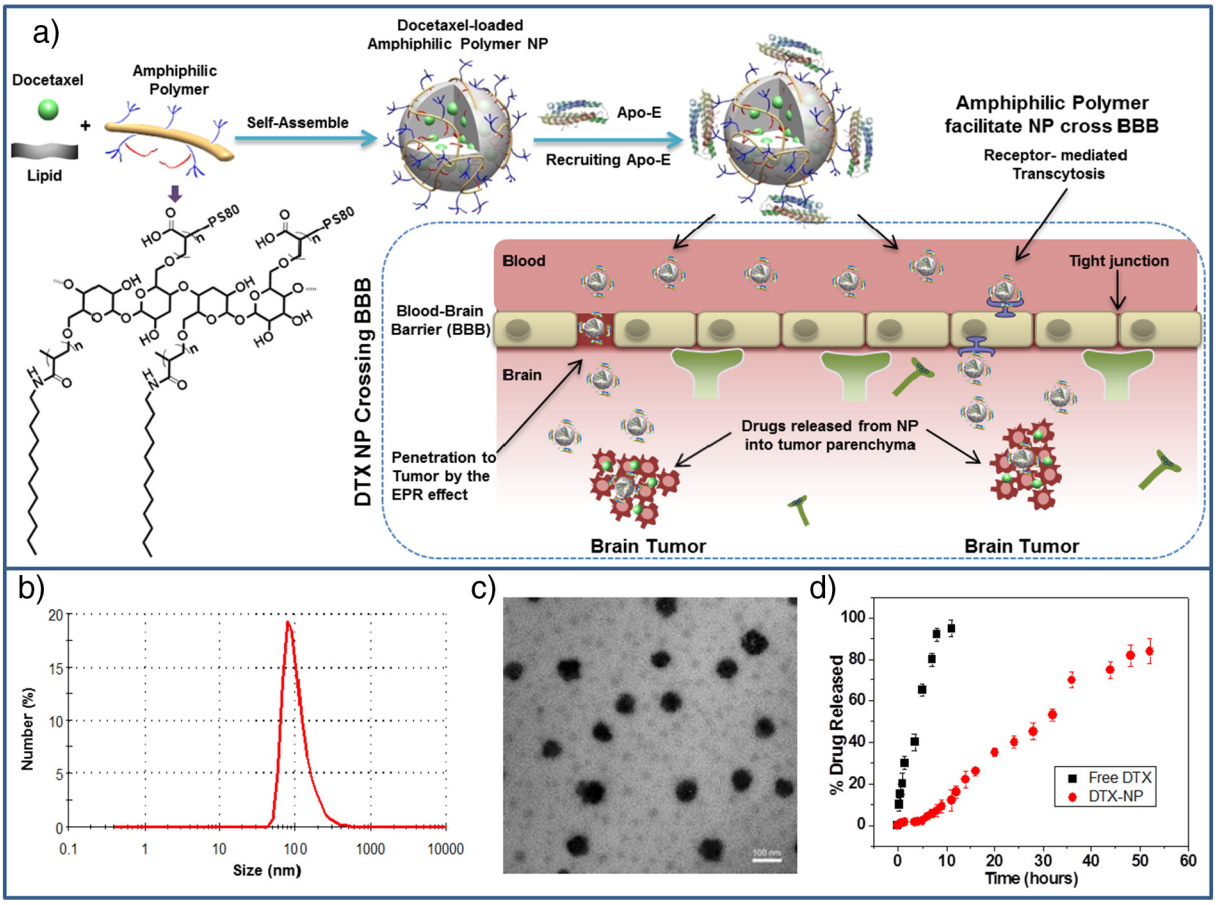

Fig. 1. a) Schematic illustration of DTX-NP formation from the amphiphilic terpolymer, recruitment of Apo-E, and proposed enhanced permeability and retention (EPR)/transcytosis mechanism for overcoming the BBB. b–d) Properties of DTX-NPs made from 10% dodecylamine grafted polymer: b) particle size distribution, c) TEM image (scale bar = 100 nm), and d) *in vitro* release of free DTX and DTX from the DTX-NPs determined by a dialysis method (data presented as means ± SD, n = 3).

content were found to exhibit smaller particle size, narrower size distributions, higher DTX encapsulation efficiency and higher DTX loading content (Table 1), conceivably due to stronger hydrophobic interactions between the amphiphilic polymer, lipid domain and hydrophobic drug. DTX-NP made from the polymer with 10% dodecyl content had an average particle diameter of 100.1 ± 2.6 nm, polydispersity of 0.17, zeta potential of −48 mV, loading efficiency of 98.2 ± 1.0%, and loading content of 6.8 ± 1.4% (Fig. 1b, c; Table 1). Based on these observations, all subsequent studies were performed using DTX-NP with 10% dodecyl content without further specification.

Transmission electron micrographs of the DTX-NP (Fig. 1c) showed spherical shape and relatively uniform particle size. The DTX-NP were stable at 37 °C in both pH 7.4 PBS and 100% FBS for at least 72 h (Supporting information, Fig. S2). As shown in Fig. 1d, DTX-NP provided a sustained *in vitro* drug release profile for over 50 h following a brief lag time. Half of the encapsulated DTX was released within 30 h while >85% of the total encapsulated drug was released after 53 h. In contrast, free DTX in solution, encased in the same type of dialysis tube under the same experimental conditions as a reference, completed the release within 10 h. This result indicates that the sustained release profile of DTX-NP measured by the dialysis method is mainly controlled by drug release from the NP into the medium inside dialysis tube, rather than by the permeation of free drug across the dialysis tube membrane into the release medium outside the tube [55]. Sustained drug release of DTX-NP following the initial lag is a desirable characteristic for therapeutic application as the NP would not release noticeable amount of drug prematurely before arrival at the tumor.

3.2. DTX-NP exhibit rapid cell uptake and enhance cytotoxicity in triple negative human breast cancer cells

In vitro kinetics of NP uptake by MDA-MB-231-luc breast cancer cells was studied using fluorescence microscopy. The Nile red-loaded NP (NR-DTX-NP) enabled *in vitro* fluorescence detection and quantification of cellular uptake. Rapid NP uptake into the cell cytoplasm was observed, with 50% of the NP being taken up by the cancer cells after 20 min (Fig. 2a, b). *In vitro* cytotoxicity studies were conducted using the MTT assay. The Blank NPs were found to be non-cytotoxic to the cells at concentrations up to 200 μg/L while DTX-NP exhibited enhanced cytotoxic effect against the MDA-MB-231-luc cells compared to free DTX (DTX-NP: IC_{50} = 80.7 ± 1.2 μg/L; Free DTX: IC_{50} = 93.9 ± 3.5 μg/-L(Fig. 2c)). This enhanced cytotoxicity may be attributed to the effective uptake of the NP, increased DTX solubility and sustained release of DTX from DTX-NPs in the cytoplasm. The elevated intracellular drug concentration could significantly magnify the anticancer efficacy [37].

3.3. PS 80-containing amphiphilic polymer nanoparticles deliver BBB-impermeable dye into healthy brain

To test our hypothesis that only PS 80-containing NPs are able to extravasate brain microvessels and deliver cargos across the BBB, BBB-impermeable fluorescent dye Hoechst 33342 was loaded in FA-labeled NP with or without covalently bound PS 80. The NP were administered intravenously to healthy SCID mice and allowed to circulate for up to 2 h. Confocal laser scanning microscopy was used to examine brain tissue

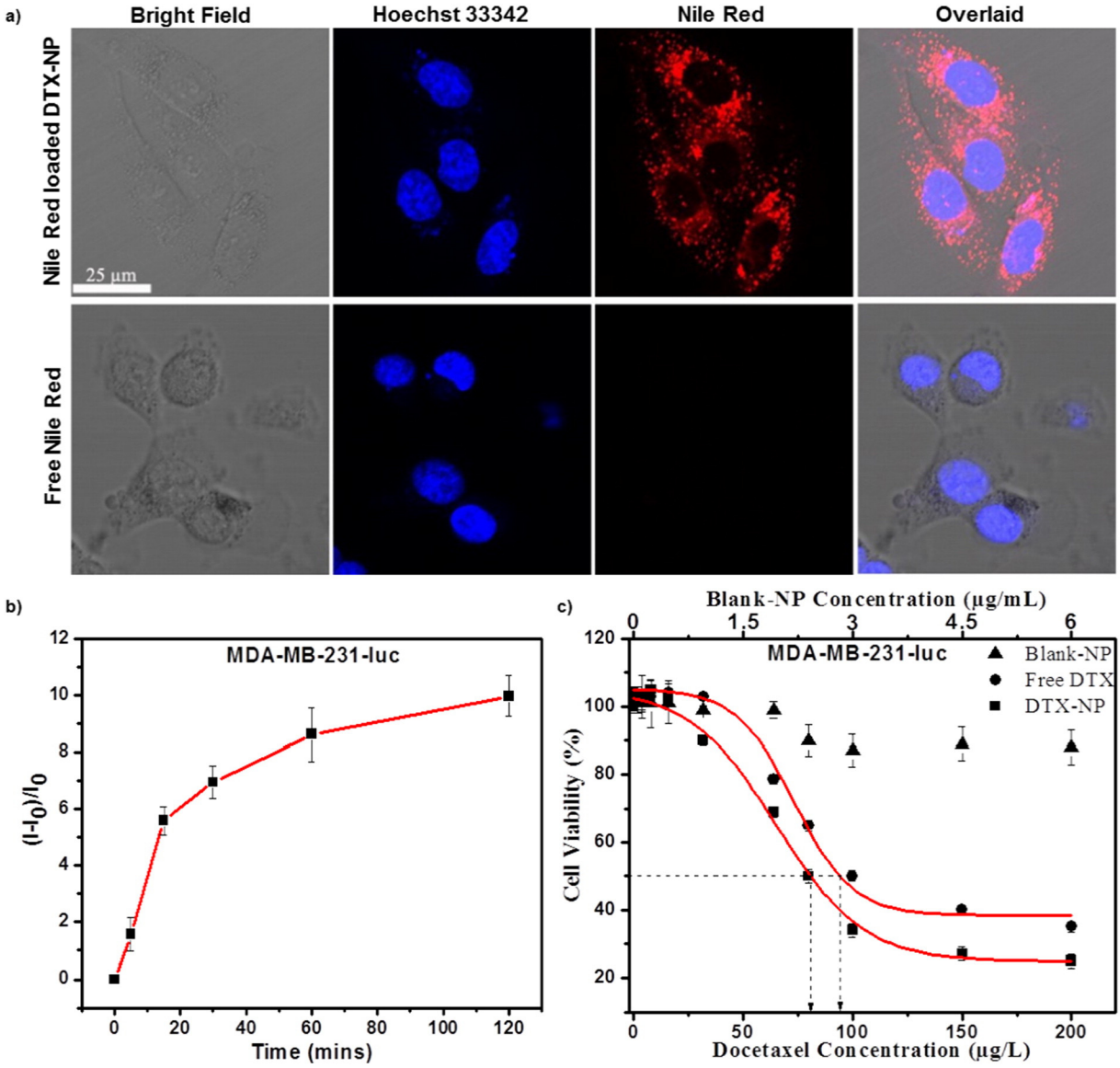

Fig. 2. Uptake of fluorescence dye-loaded DTX-NP by triple negative human breast cancer cell MDA-MB-231-luc. a) Fluorescence microscopy image at 2 h following treatment. Bright field, cell nuclei stained with Hoechst 33,342 (blue), DTX-NP stained with Nile Red (red) and overlays are shown. b) Kinetics of dye-loaded DTX-NP uptake in MDA-MB-231-luc over a 2 h period (I_0: the fluorescence intensity of cells incubated with medium; I: the fluorescence intensity of cells incubated with NR-DTX-NP). c) Cytotoxicity of Blank NP, Free DTX and DTX NP against MDA-MB-231 cells after 24 h of incubation. From the data fitting corresponding IC_{50} values were obtained (DTX-NP: $IC_{50} = 80.7 \pm 1.2$ μg/L; Free DTX: $IC_{50} = 93.9 \pm 3.5$ μg/L). Data presented as mean ± SD (n = 3). (For interpretation of the references to color in this figure legend, the reader is referred to the web version of this article.)

sections for cell nuclei stained with Hoechst 33342 (blue) in relation to brain vasculature, labeled with Texas Red-dextran (red) (Supporting information, Fig. S3). Intravenous administration of free Hoechst 33342 or Hoechst 33342-loaded NP without PS 80 could only stain nuclei of blood vessel-associated cells (blue), leaving cells away from blood vessels unstained (Supporting information, Fig. S3). In addition, PS 80-absent NPs (green) were confined within the blood vessel lumen and were absent from the brain parenchyma. In contrast, the PS 80-containing NP (green) were able to extravasate from the blood vessel lumen, enter the brain parenchyma, and to deliver the dye to cells located away from brain capillaries (blue).

These results suggest that covalently bound PS 80 plays an important role in NP entry into the brain, as only the PS-80 containing NP were able to penetrate the BBB entering intact normal brain. It has been reported that coating NP with PS 80 leads to enhanced adsorption of apolipoprotein-E (Apo-E) in the blood onto the particle surface, and the presence of Apo-E promotes NP internalization in the brain capillary endothelial cells *via* members of the LDL receptor family expressed by these cells [56,57]. Therefore, it is perceivable that a similar mechanism is responsible for the uptake of the PS 80-containing amphiphilic polymer NP by the brain capillary endothelial cells and transcytosis to the outside of the blood vessels.

3.4. Biodistribution and brain tumor accumulation of DTX-NP

The MDA-MB-231-luc-D3H2LN triple-negative human breast cancer cell line, derived from spontaneous lymph node metastases from mammary fat pad tumors, was selected to establish the brain metastasis model due to its aggressive proliferation and infiltration behavior leading to the formation of multiple metastatic lesions throughout the brain (Fig. S1), resembling breast cancer metastases in humans [58]. Intracranial injection of the cells resulted in the formation of numerous small sized tumor lesions throughout the brain, including the cortex and subcortex (Fig. S1, Fig. 3), similar to those found in BMBC models established using intracardiac injection of MDA-MB-231-BR cells [59]. Tumor growth was monitored in live animals using bioluminescence

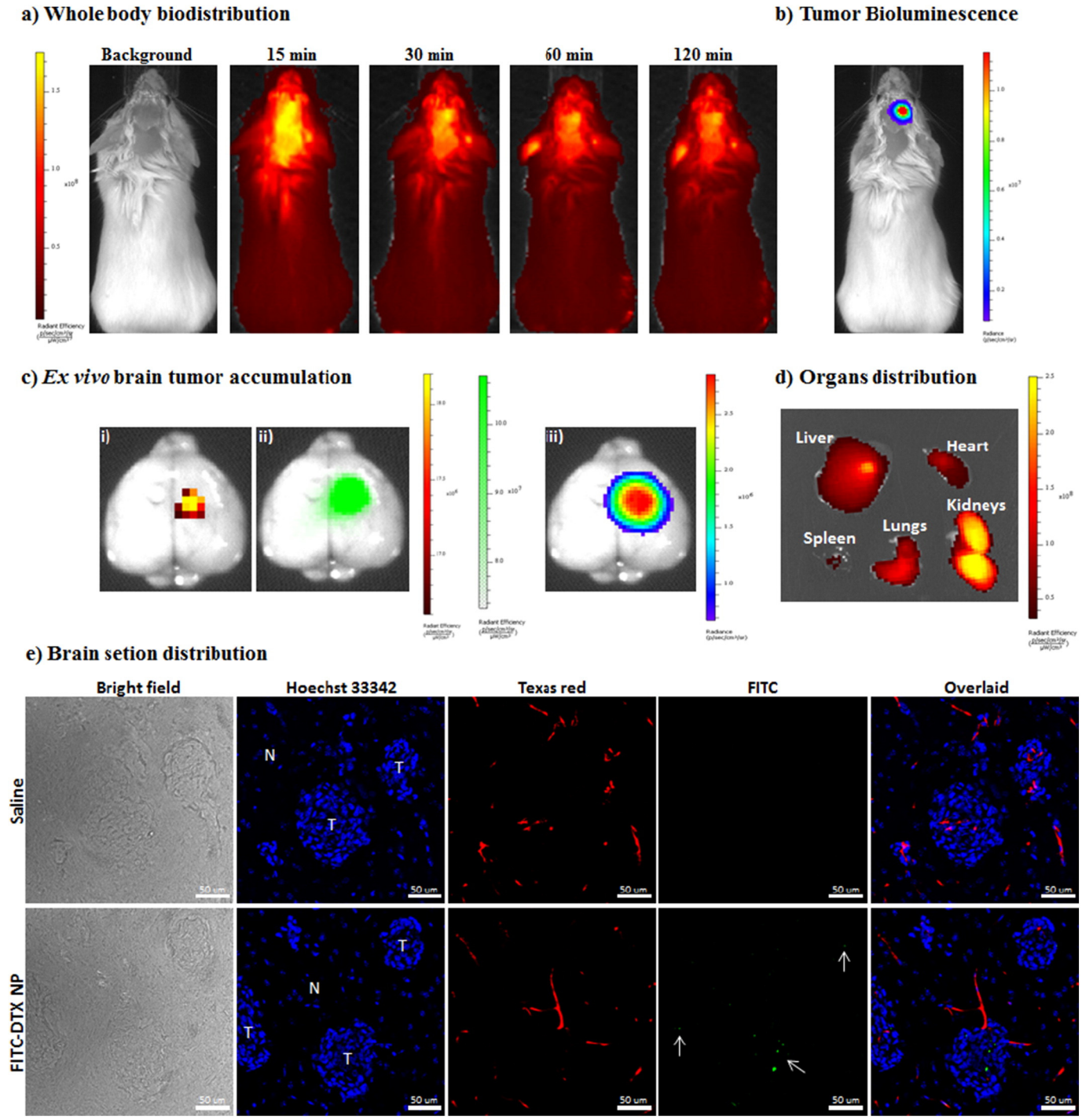

Fig. 3. a–d) Whole body images of live mice with brain tumor at various times and *ex vivo* images of organs: a) Representative fluorescence images showing tumor accumulation of HF 750- and FA-labeled DTX-NPs; b) bioluminescence image of luciferase-expressing-tumor cells; c) *Ex vivo* image of fluorescence signals of NP (i: HF 750 filter; ii: FITC filter) in the brain tumor region; (iii) bioluminescence signals of brain tumor region. d) Representative fluorescence images of NP in different organs. e) Confocal microscopic images of brain sections taken from mice-bearing brain metastases 2 h after i.v. injection of saline (top panel) or FA-labeled DTX NP (green, bottom panel). Texas red-dextran (red) was administered to the mice i.v. 15 min before euthanasia. Hoechst 33342-stained cell nuclei shown in blue (T: brain tumor area; N: normal area without tumor). Arrows point to representative FA-labeled DTX-NP away from blood vessels and accumulated into microscopic tumor lesions. Scale = 50 μm for all images. (For interpretation of the references to color in this figure legend, the reader is referred to the web version of this article.)

imaging of the luciferase-transfected tumor cells following intraperitoneal administration of luciferin. The brain tumors were allowed to grow for two weeks following intracranial inoculation.

Accumulation of HF 750- and FA-labeled DTX-NP at the brain tumor site is evidenced by the co-localization of fluorescence signal from DTX-NP with the bioluminescence signal of brain tumor cells *in vivo* (Fig. 3a, b). The NP remained at the tumor site for at least two hours following treatment. Immediate *ex vivo* fluorescence and bioluminescence imaging of the dissected brain 2 h after DTX-NP injection confirmed these results (Fig. 3c). Laser scanning confocal microscopy of the tumor-bearing

brain tissue sections revealed that the FA-labeled DTX-NP (green) were able to extravasate from the blood vessel lumen (red) and accumulate within tumor lesions in the brain (Fig. 3e).

NP accumulation in the major organs following a single i.v. injection of HF 750-labeled DTX-NP was determined by *ex vivo* fluorescence imaging (Fig. 3d, Supporting information, Fig. S4). DTX-NP initially accumulated in the kidneys, lungs and the liver, and were significantly removed from these organs and cleared from the blood within 6 h. The relatively high fluorescence intensity in the kidneys could be ascribed to the released HF 750-bound polymer chains that undergo elimination through kidneys.

3.5. DTX-NP prolong blood circulation time of DTX and increase its brain bioavailability compared to Taxotere®

The concentration of DTX in the perfused brains of healthy mice was quantified using LC-MS/MS following i.v. injection of DTX-NP or Taxotere® (20 mg/kg DTX) (Fig. 4a). DTX was found to be present in the brain of healthy mice at low concentrations (<100 ng/g), similar to values reported in previous studies [60,61], as early as 15 min following i.v. injection of Taxotere®. Treatment with an identical dose of DTX-NP resulted in a 3.6-fold higher DTX concentration in the brain of healthy mice 15 min after injection. These results demonstrate that DTX encapsulated within the NP were able to cross the intact BBB of healthy mice within 15 min after i.v. injection leading to enhanced accumulation of DTX in the central nervous system compared Taxotere®.

The mechanism of DTX entry into the healthy brain following treatment with Taxotere® is unclear; though it may be related to the high PS 80 content (80–260 mg/mL PS 80) in this formulation [62]. We detected micelles in Taxotere® diluted in DDIW by dynamic light scattering with a number average particle size of 7.8 ± 0.3 nm and a polydispersity index of 0.18 ± 0.11 (Supporting information, Fig. S5). If the micelles were actually maintained in the blood circulation, they may enter the tumor lesion where the enhanced permeability and retention (EPR) effect may operate. Since clinical treatment with high levels of PS 80 has been associated with unpredictable hypersensitivity reactions [63], our DTX-NP formulation may mitigate this problem by significantly reducing PS 80 content to only 10 mg/mL PS 80.

Compared to treatment in healthy mice, intravenous injection of both Taxotere® and DTX-NP to mice with brain tumors resulted in > 2-fold higher DTX concentrations in the tumor-bearing brain 15 min after injection (Fig. 4a). This phenomenon may be attributed to the compromised BBB structure typical of brain tumor lesions, leading to higher drug permeability into the brain [64–66]. Previously Lockman et al. demonstrated that while the BBB in >89% of BMBC lesions were more permeable to chemotherapy drugs, drug accumulation at cytotoxic concentrations was only achieved in roughly 10% of these lesions [10]. Therefore it is thought that the compromised BBB remains a significant barrier to drug delivery to brain metastases despite its enhanced permeability. Intravenous injection of DTX-NP to mice with brain tumors with resulted in a 2.7-fold higher DTX concentration in the tumor-bearing brain 15 min following treatment compared to treatment with an equivalent dose of Taxotere® (Fig. 4a). A time course study in mice

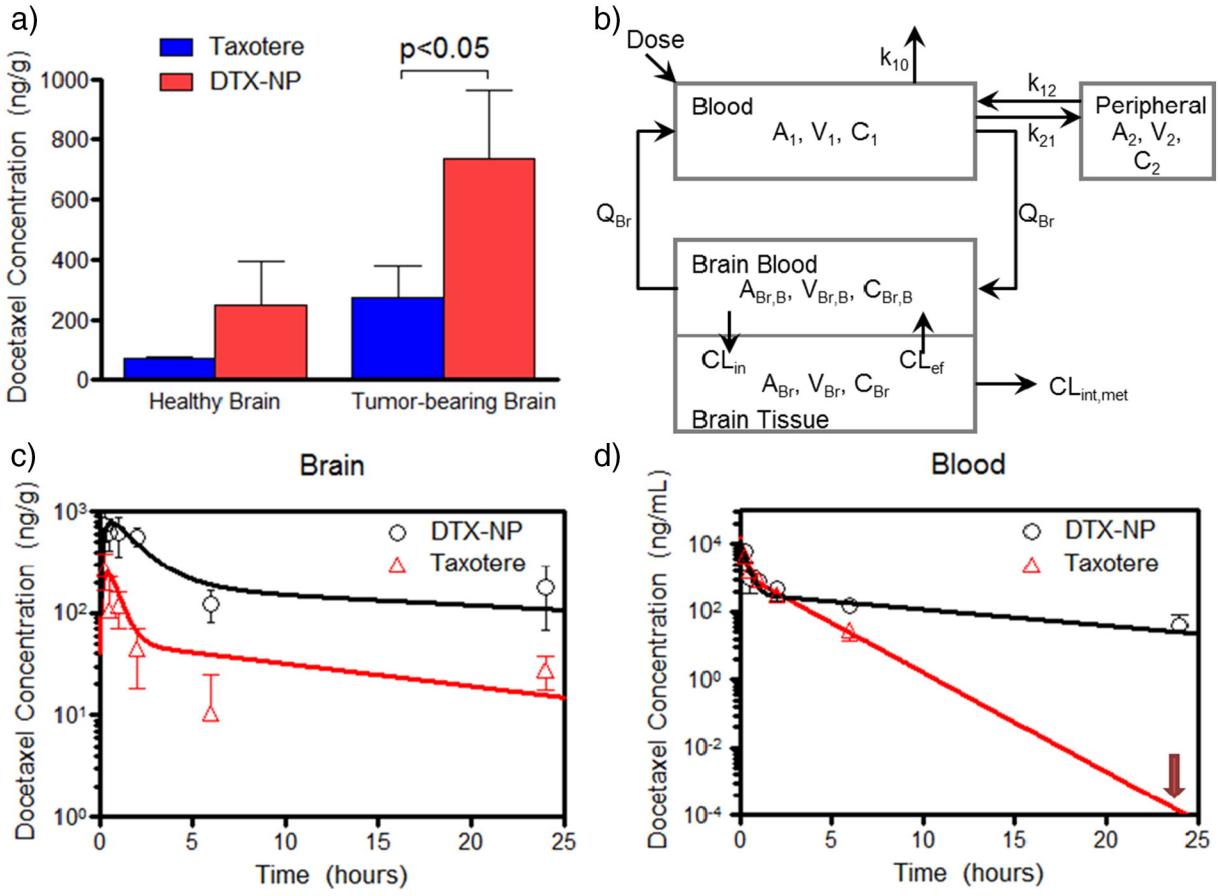

Fig. 4. Pharmacokinetics of DTX-NPs and Taxotere® in brain and whole blood. a) The concentration of DTX in healthy brains and tumor-bearing brains at 15 min after i.v. injection. b) Illustration of a semi-PBPK model for DTX disposition. All parameters are defined in the main text and in the supplementary material. Concentration profiles of DTX in brain (c) and in blood (d) after i.v. injection of DTX-NP or Taxotere® (symbols are measured values, lines are fitted data). DTX concentration in the blood of Taxotere® treated mice at 24 h was below the detection limit. Therefore a value of zero was used for PK modeling (Red Arrow). All measured data in a, c, d are the mean ± SD (n = 3). (For interpretation of the references to color in this figure legend, the reader is referred to the web version of this article.)

Table 2
Fitted pharmacokinetic parameters to LC-MS/MS data for DTX-NP and Taxotere® in whole blood and brains of tumor-bearing mice after a single intravenous administration of 20 mg/kg DTX (n = 3).

	DTX-NP	Taxotere®	DTX-NP/Taxotere®
Blood			
$T_{1/2\ term}$ (h)	6.35	1.16	5.47
$AUC_{0-24\ h}$ (ng·h/mL)[a]	5.95×10^3	4.43×10^3	1.34
CL (mL/h)	64.7	90.2	0.71
V_1 (mL)	32.9	25.7	1.28
Brain			
$T_{1/2\ term}$ (h)	31.5	13.7	2.30
$T_{1/2\ redis}$ (h)	2.17	0.68	3.24
$AUC_{0-24\ h}$ (ng·h/g)[a]	4.83×10^3	0.95×10^3	5.09
C_{max} (ng/g)	0.78×10^3	0.25×10^3	3.11
T_{max} (h)	0.64	0.43	1.49
$AUC_{brain,\ 0-24\ h}$ / $AUC_{blood,0-24\ h}$	0.81	0.21	3.86

$T_{1/2\ term}$ represents the elimination half-life.
$T_{1/2\ redis}$ represents redistribution the half-life in the brain, between C_{max} and the terminal elimination phase.
T_{max} represents the time to reach C_{max}.
CL is the total body clearance determined according to CL = dose / $AUC_{0-\infty}$.
C_{max} is the peak concentration of DTX in the brain after administration.
V_1 is defined as the volume of central compartment.
[a] $AUC_{0-24\ h}$ is area under the curve from time 0 to 24 h. The mean (n = 3) of all data points were used for calculation.

with brain tumors further demonstrated that DTX-NP treatment resulted in markedly higher levels of DTX in the brain at all time points tested as compared to treatment with Taxotere® (Fig. 4c), indicating that DTX-NP enhanced drug delivery to brain metastases.

Pharmacokinetic modeling was used to quantitatively analyze the influence of formulation (*i.e.*, DTX-NP *vs.* Taxotere®) on the DTX pharmacokinetics (Fig. 4b) with good precision as evidenced by low coefficient of variation (Supporting information Table S1). Physiological parameters and fitted results are summarized in the Supporting information in Tables S1 and S2, respectively. DTX was not detected in the blood 24 h after Taxotere® injection; therefore a value of zero was used at this time point for pharmacokinetic modeling.

The blood DTX concentration profiles after a single i.v. dose of Taxotere® or DTX-NP (20 mg/kg DTX) showed a bi-exponential decay of DTX for both formulations (Fig. 4d). Taxotere® was quickly eliminated from the blood within 24 h after injection. In contrast, DTX-NP extended DTX circulation time and significantly increased total drug exposure over time in the blood with a 5.5-fold increase in blood terminal half-life ($T_{1/2\ term}$), a 1.3-fold increase in blood $AUC_{0-24\ h}$, and 29% decrease in total body clearance (CL) compared to Taxotere® (Table 2). The favorable pharmacokinetics obtained by NP formulation is consistent with other NP formulations [67].

Treatment of mice bearing brain tumor with DTX-NP resulted in a 3-fold higher C_{max} and a 5.1-fold higher $AUC_{0-24\ h}$ in the brain compared to treatment with an equivalent dose of Taxotere® (Table 2). Transport of PS 80-containing NP across the BBB is thought to occur *via* surface adsorption of apolipoprotein E (ApoE) in plasma followed by receptor-mediated transcytosis through brain microvessel endothelial cells [31, 54]. However, increased permeability of the BBB at the tumor site may also play a significant role for large-sized tumor lesions [64–66]. A redistribution phase was observed between C_{max} and the terminal elimination phase in the brain after treatment with DTX-NP and Taxotere®. The half-life of redistribution phase ($T_{1/2\ redis}$) in the brain was 3.2-fold longer in the DTX-NP-treated mice compared to the Taxotere® group, suggesting that the NP likely bypass efflux pumps on the BBB. It should be noted that measured drug concentrations in brain tumor lesions may in fact be much higher than the measured DTX levels, since these levels are averaged over the entire tumor-bearing brain which includes a large amount of non-diseased brain tissue.

3.6. Ex vivo fluorescence imaging of nanoparticles as an indicator of DTX distribution kinetics

To investigate the role of the nanocarrier in drug pharmacokinetics in the brain (Fig. 5a) and blood (Fig. 5b), we measured the time-dependent fluorescence intensity of the NP carriers by *ex vivo* fluorescence imaging, and compared it to the kinetics of DTX concentration determined by LC-MS/MS. PK parameters related to the rates of NP and drug disposition were extracted from the fluorescence and drug concentration

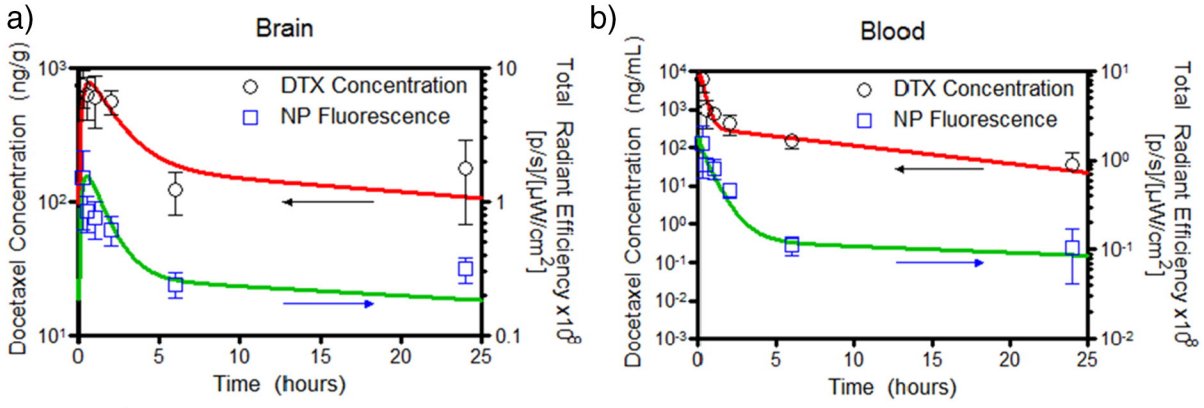

c)

	DTX concentration	NP fluorescence	DTX/fluorescence
Brain:			
T_{max} (h)	0.64	0.51	1.25
$T_{1/2\ redis}$ (h)	2.2	1.5	1.47
$T_{1/2\ term}$ (h)	31.5	43.2	0.73
Blood:			
$T_{1/2\ term}$ (h)	6.35	42	0.15

Fig. 5. a) Comparison of DTX concentration (determined by LC-MS/MS) and *ex vivo* NP fluorescence intensity *versus* time after a single i.v. injection of HF750-labeled DTX-NPs (20 mg/kg DTX) in the brain (b) and whole blood (c) of tumor-bearing mice. (d) Fitted pharmacokinetic parameters of HF750-labeled DTX-NP and DTX-NP in whole blood and brain. All data represent the mean ± SD (n = 3).

profiles respectively, and the ratio of these terms (average fluorescence intensity/drug concentration) was calculated to aid comparison between the two detection methods (Fig. 5c). The fluorescence signal profile of the NP and concentration profile of DTX in the brain were found to be similar as indicated by a near-unity of T_{max}, $T_{1/2\ redist}$ and $T_{1/2\ term}$ NP drug-to-fluorescence ratios. This finding suggests that *ex vivo* fluorescence imaging of the dye-labeled NP carrier is a good indicator of DTX accumulation kinetics in the brain for our DTX-NP formulation and that DTX entry into the brain is likely facilitated by NP transport. In contrast, the pharmacokinetics of circulating NP and blood DTX concentrations were dissimilar with the NP carrier circulating for a longer period of time ($T_{1/2\ term,\ DTX}$ / $T_{1/2\ term,\ NP\ fluorescence}$ = 0.15) than DTX in the blood. This suggests that any DTX released from the NP during circulation is rapidly cleared from the body, presumably due to its small molecular size compared to intact NP. Therefore *ex vivo* NP fluorescence signal is a poor indicator of circulating DTX concentration in the blood.

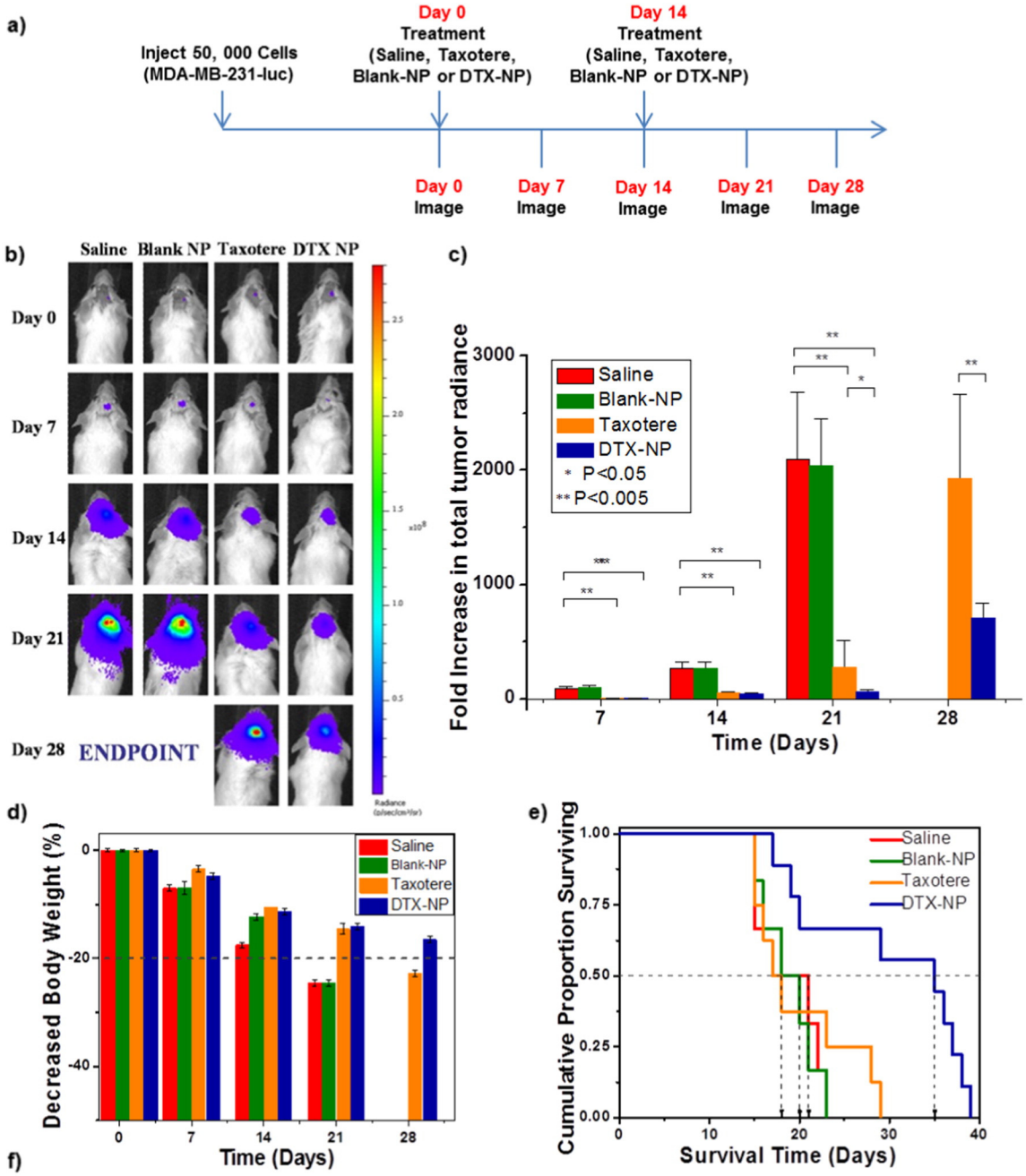

f)

Treatment Groups	Mean Survival Time (Days)	Median Survival Time (Days)	Tumor Growth Delay (TGD%)
Saline (n=6)	19±4	21	/
Blank-NP (n=7)	18±3	20	-5.3
Taxotere® (n=8)	20±6	18	5.3
DTX-NP (n=9)	30±9	35	57.9

Fig. 6. Inhibition of brain tumor growth and animal survival. a) Treatment and imaging schedule for tumor-bearing mice injected with saline (n = 6), blank NP (n = 7), Taxotere® (20 mg/kg DTX, n = 8), or DTX-NP (20 mg/kg DTX, n = 9). b) *In vivo* images of brain tumor bioluminescence over a 28 day period. c) Fold increase in the total tumor radiance. d) Body weight and e) Kaplan–Meier survival curve of tumor-bearing mice following treatment. f) Effect of treatment on median survival time and tumor growth delay of tumor bearing mice. All data presented as mean ± SD.

3.7. DTX-NP inhibit growth of brain metastases and extend survival compared to Taxotere®

To evaluate therapeutic efficacy of DTX-NP, BMBC-bearing mice were injected with an equivalent dose of DTX-NP (20 mg/kg DTX), Taxotere (20 mg/kg DTX), saline or blank NP on day 0 and day 14 (Fig. 6a). The general health, weight, and size of brain tumors, measured using *in vivo* fluorescence imaging, were monitored over a period of 40 days. Brain tumor-bearing mice treated with saline or blank NP (Fig. 6) exhibited the fastest tumor growth, animal weight loss (Fig. 6b, c and d), and the shortest mean survival times at 19 and 18 days, respectively (Fig. 6e). Treatment with Taxotere® extended the mean survival time to 20 days with a similar median survival time of 18 days (Fig. 6f). This is not surprising given the innate ability of Taxotere® to enter the brain at low concentrations [60,61], possibly due to the high PS 80 content of the Taxotere® as discussed above. In contrast, DTX-NP treatment delayed tumor growth by 11-fold (57.9% *vs*. 5.3%), and prolonged the median survival time of tumor-bearing mice by 1.9-fold compared to an equivalent dose of Taxotere®, and 1.7-fold compared to saline control (Fig. 6f). The improved therapeutic effect of the DTX-NPs may be due to a combination of the ability of the NP to actively enter the brain through receptor-mediated transcytosis, passive accumulation at sites of impaired blood-tumor vasculature, and sustained release of DTX from the NP which have accumulated at the tumor site [31].

3.8. DTX-NP treatment did not induce histological changes of main organs

To evaluate possible toxicity in the major organs resulting from DTX-NP treatment, histological tissue sections stained with hematoxylin and eosin were prepared from the lungs, liver, kidneys and heart of tumor-bearing mice treated with 20 mg/kg DTX-NP or Taxotere® at the end point. The tissue sections showed no histological abnormalities in any of the major organs as compared to saline and Blank-NP controls (Supporting information Fig. S6). Thus DTX-NP exhibited improved therapeutic efficacy compared to Taxotere® treatment groups without inducing histological changes in the major organs at the administered dosing level and regimen.

4. Conclusions

In summary, we have successfully prepared DTX-loaded amphiphilic polymer NP by a one-step self-assembly method and demonstrated their ability to cross the BBB *via* systemic administration in healthy mice and in a BMBC mouse model. The DTX-NPs accumulated within tumor lesions, effectively inhibited tumor growth, and increased median survival compared to an equivalent dose of clinically used DTX solution formulation (Taxotere®). Pharmacokinetic modeling showed quantitatively that NP encapsulation of DTX increased drug bioavailability in the brain and prolonged blood circulation compared to Taxotere®. The similarity between the DTX pharmacokinetics and the kinetics of *ex vivo* NP fluorescence intensity in the brain suggested that DTX entry into the brain was likely facilitated by NP transport across the BBB, and more generally that *ex vivo* imaging of NP fluorescence is a potential indicator of drug disposition in the brain. The results of this work suggest that the developed DTX-NP formulation is a promising NP system for treatment of brain metastases of TNBC.

Acknowledgments

The authors gratefully thank the Canadian Institutes of Health Research (CIHR) for the Proof-of-Principle grant and the Natural Sciences and Engineering Research Council (NSERC) of Canada for the Discovery and the Equipment Grants to X.Y. Wu; the scholarships from NSERC of Canada, Ontario Graduate Scholarship, and the Department of Pharmaceutical Sciences at the University of Toronto to J. Li and T. Zhang. The authors also thank the Spatio-Temporal Targeting and Amplification of Radiation Response (STTARR) program and its affiliated funding agencies; Lily Morikawa and Hibret Addisu at the Pathology Core of the Centre (Lunfeld-Tanenbaum Research Institute) for Modeling Human Disease; Michelle Young and Dr. Matthew Forbes at the Advanced Instrumentation for Molecular Structure (AIMS) Mass Spectrometry Laboratory (Department of Chemistry, University of Toronto).

Appendix A. Supplementary data

Supplementary data to this article can be found online at http://dx.doi.org/10.1016/j.jconrel.2016.12.019.

References

[1] I. Witzel, L. Oliveira-Ferrer, K. Pantel, V. Muller, H. Wikman, Breast cancer brain metastases: biology and new clinical perspectives, Breast Cancer Res. 18 (2016) 8.
[2] M.R. Quigley, O. Fukui, B. Chew, S. Bhatia, S. Karlovits, The shifting landscape of metastatic breast cancer to the CNS, Neurosurg. Rev. 36 (2013) 377–382.
[3] S.A. Chikarmane, S.H. Tirumani, S.A. Howard, J.P. Jagannathan, P.J. DiPiro, Metastatic patterns of breast cancer subtypes: what radiologists should know in the era of personalized cancer medicine, Clin. Radiol. 70 (2015) 1–10.
[4] E. Lim, N.U. Lin, Updates on the management of breast cancer brain metastases, Oncology 28 (2014) 572–578.
[5] D. Palmieri, J.L. Bronder, J.M. Herring, T. Yoneda, R.J. Weil, A.M. Stark, R. Kurek, E. Vega-Valle, L. Feigenbaum, D. Halverson, A.O. Vortmeyer, S.M. Steinberg, K. Aldape, P.S. Steeg, Her-2 overexpression increases the metastatic outgrowth of breast cancer cells in the brain, Cancer Res. 67 (2007) 4190–4198.
[6] N.U. Lin, E. Claus, J. Sohl, A.R. Razzak, A. Arnaout, E.P. Winer, Sites of distant recurrence and clinical outcomes in patients with metastatic triple-negative breast cancer: high incidence of central nervous system metastases, Cancer 113 (2008) 2638–2645.
[7] W. Löscher, H. Potschka, Blood-brain barrier active efflux transporters: ATP-binding cassette gene family, NeuroRx 2 (2005) 86–98.
[8] H.L. Wong, X.Y. Wu, R. Bendayan, Nanotechnological advances for the delivery of CNS therapeutics, Adv. Drug Deliv. Rev. 64 (2012) 686–700.
[9] W.M. Pardridge, The blood-brain barrier: bottleneck in brain drug development, NeuroRx 2 (2005) 3–14.
[10] P.R. Lockman, R.K. Mittapalli, K.S. Taskar, V. Rudraraju, B. Gril, K.A. Bohn, C.E. Adkins, A. Roberts, H.R. Thorsheim, J.A. Gaasch, S. Huang, D. Palmieri, P.S. Steeg, Q.R. Smith, Heterogeneous blood-tumor barrier permeability determines drug efficacy in experimental brain metastases of breast cancer, Clin. Cancer Res. 16 (2010) 5664–5678.
[11] D.R. Groothuis, The blood-brain and blood-tumor barriers: a review of strategies for increasing drug delivery, Neuro-Oncology 2 (2000) 45–59.
[12] T. Siegal, R. Rubinstein, F. Bokstein, A. Schwartz, A. Lossos, E. Shalom, R. Chisin, J.M. Gomori, In vivo assessment of the window of barrier opening after osmotic blood-brain barrier disruption in humans, J. Neurosurg. 92 (2000) 599–605.
[13] B. Gril, D. Palmieri, J.L. Bronder, J.M. Herring, E. Vega-Valle, L. Feigenbaum, D.J. Liewehr, S.M. Steinberg, M.J. Merino, S.D. Rubin, P.S. Steeg, Effect of lapatinib on the outgrowth of metastatic breast cancer cells to the brain, J. Natl. Cancer Inst. 100 (2008) 1092–1103.
[14] B. Gril, D. Palmieri, Y. Qian, T. Anwar, D.J. Liewehr, S.M. Steinberg, Z. Andreu, D. Masana, P. Fernandez, P.S. Steeg, F. Vidal-Vanaclocha, Pazopanib inhibits the activation of PDGFRbeta-expressing astrocytes in the brain metastatic microenvironment of breast cancer cells, Am. J. Pathol. 182 (2013) 2368–2379.
[15] B. Gril, D. Palmieri, Y. Qian, D. Smart, L. Ileva, D.J. Liewehr, S.M. Steinberg, P.S. Steeg, Pazopanib reveals a role for tumor cell B-Raf in the prevention of HER2+ breast cancer brain metastasis, Clin. Cancer Res. 17 (2011) 142–153.
[16] D. Palmieri, P.R. Lockman, F.C. Thomas, E. Hua, J. Herring, E. Hargrave, M. Johnson, N. Flores, Y. Qian, E. Vega-Valle, K.S. Taskar, V. Rudraraju, R.K. Mittapalli, J.A. Gaasch, K.A. Bohn, H.R. Thorsheim, D.J. Liewehr, S. Davis, J.F. Reilly, R. Walker, J.L. Bronder, L. Feigenbaum, S.M. Steinberg, K. Camphausen, P.S. Meltzer, V.M. Richon, Q.R. Smith, P.S. Steeg, Vorinostat inhibits brain metastatic colonization in a model of triple-negative breast cancer and induces DNA double-strand breaks, Clin. Cancer Res. 15 (2009) 6148–6157.
[17] Y. Qian, E. Hua, K. Bisht, S. Woditschka, K.W. Skordos, D.J. Liewehr, S.M. Steinberg, E. Brogi, M.M. Akram, J.K. Killian, D.C. Edelman, M. Pineda, S. Scurci, Y.Y. Degenhardt, S. Laquerre, T.A. Lampkin, P.S. Meltzer, K. Camphausen, P.S. Steeg, D. Palmieri, Inhibition of polo-like kinase 1 prevents the growth of metastatic breast cancer cells in the brain, Clin. Exp. Metastasis 28 (2011) 899–908.
[18] D.P. Fitzgerald, D.L. Emerson, Y. Qian, T. Anwar, D.J. Liewehr, S.M. Steinberg, S. Silberman, D. Palmieri, P.S. Steeg, TPI-287, a new taxane family member, reduces the brain metastatic colonization of breast cancer cells, Mol. Cancer Ther. 11 (2012) 1959–1967.
[19] R.K. Mittapalli, X. Liu, C.E. Adkins, M.I. Nounou, K.A. Bohn, T.B. Terrell, H.S. Qhattal, W.J. Geldenhuys, D. Palmieri, P.S. Steeg, Q.R. Smith, P.R. Lockman, Paclitaxel–hyaluronic nanoconjugates prolong overall survival in a preclinical brain metastases of breast cancer model, Mol. Cancer Ther. 12 (2013) 2389–2399.
[20] D.T. Wiley, P. Webster, A. Gale, M.E. Davis, Transcytosis and brain uptake of transferrin-containing nanoparticles by tuning avidity to transferrin receptor, Proc. Natl. Acad. Sci. U. S. A. 110 (2013) 8662–8667.

[21] J. Niewoehner, B. Bohrmann, L. Collin, E. Urich, H. Sade, P. Maier, P. Rueger, J.O. Stracke, W. Lau, A.C. Tissot, H. Loetscher, A. Ghosh, P.O. Freskgard, Increased brain penetration and potency of a therapeutic antibody using a monovalent molecular shuttle, Neuron 81 (2014) 49–60.
[22] Y.J. Yu, Y. Zhang, M. Kenrick, K. Hoyte, W. Luk, Y. Lu, J. Atwal, J.M. Elliott, S. Prabhu, R.J. Watts, M.S. Dennis, Boosting brain uptake of a therapeutic antibody by reducing its affinity for a transcytosis target, Sci. Transl. Med. 3 (2011) 84ra44.
[23] S. Wagner, A. Zensi, S.L. Wien, S.E. Tschickardt, W. Maier, T. Vogel, F. Worek, C.U. Pietrzik, J. Kreuter, H. von Briesen, Uptake mechanism of ApoE-modified nanoparticles on brain capillary endothelial cells as a blood-brain barrier model, PLoS One 7 (2012), e32568. .
[24] J. Kreuter, Drug delivery to the central nervous system by polymeric nanoparticles: what do we know? Adv. Drug Deliv. Rev. 71 (2014) 2–14.
[25] K. Ulbrich, T. Knobloch, J. Kreuter, Targeting the insulin receptor: nanoparticles for drug delivery across the blood-brain barrier (BBB), J. Drug Target. 19 (2011) 125–132.
[26] X. Yi, D.S. Manickam, A. Brynskikh, A.V. Kabanov, Agile delivery of protein therapeutics to CNS, J. Control. Release 190 (2014) 637–663.
[27] A. Jain, S.K. Jain, Ligand-appended BBB-targeted nanocarriers (LABTNs), Crit. Rev. Ther. Drug 32 (2015) 149–180.
[28] M.M. Patel, B.R. Goyal, S.V. Bhadada, J.S. Bhatt, A.F. Amin, Getting into the brain approaches to enhance brain drug delivery, CNS Drugs 23 (2009) 35–58.
[29] T. Patel, J.B. Zhou, J.M. Piepmeier, W.M. Saltzman, Polymeric nanoparticles for drug delivery to the central nervous system, Adv. Drug Deliv. Rev. 64 (2012) 701–705.
[30] J. Li, P. Cai, A. Shalviri, J.T. Henderson, C. He, W.D. Foltz, P. Prasad, P.M. Brodersen, Y. Chen, R. DaCosta, A.M. Rauth, X.Y. Wu, A multifunctional polymeric nanotheranostic system delivers doxorubicin and imaging agents across the blood-brain barrier targeting brain metastases of breast cancer, ACS Nano 8 (2014) 9925–9940.
[31] R.M. Koffie, C.T. Farrar, L.-J. Saidi, C.M. William, B.T. Hyman, T.L. Spires-Jones, Nanoparticles enhance brain delivery of blood–brain barrier-impermeable probes for in vivo optical and magnetic resonance imaging, Proc. Natl. Acad. Sci. U. S. A. 108 (2011) 18837–18842.
[32] S. Wohlfart, S. Gelperina, J. Kreuter, Transport of drugs across the blood-brain barrier by nanoparticles, J. Control. Release 161 (2012) 264–273.
[33] J. Kreuter, Mechanism of polymeric nanoparticle-based drug transport across the blood-brain barrier (BBB), J. Microencapsul. 30 (2013) 49–54.
[34] S.C. Steiniger, J. Kreuter, A.S. Khalansky, I.N. Skidan, A.I. Bobruskin, Z.S. Smirnova, S.E. Severin, R. Uhl, M. Kock, K.D. Geiger, S.E. Gelperina, Chemotherapy of glioblastoma in rats using doxorubicin-loaded nanoparticles, Int. J. Cancer 109 (2004) 759–767.
[35] S.A. Kulkarni, S.S. Feng, Effects of surface modification on delivery efficiency of biodegradable nanoparticles across the blood-brain barrier, Nanomedicine (London) 6 (2011) 377–394.
[36] A. Shalviri, H.K. Chan, G. Raval, M.J. Abdekhodaie, Q. Liu, H. Heerklotz, X.Y. Wu, Design of pH-responsive nanoparticles of terpolymer of poly (methacrylic acid), polysorbate 80 and starch for delivery of doxorubicin, Colloids Surf. B: Biointerfaces 101 (2013) 405–413.
[37] A. Shalviri, G. Raval, P. Prasad, C. Chan, Q. Liu, H. Heerklotz, A.M. Rauth, X.Y. Wu, pH-Dependent doxorubicin release from terpolymer of starch, polymethacrylic acid and polysorbate 80 nanoparticles for overcoming multi-drug resistance in human breast cancer cells, Eur. J. Pharm. Biopharm. 82 (2012) 587–597.
[38] H. Gao, Z. Yang, S. Cao, Y. Xiong, S. Zhang, Z. Pang, X. Jiang, Tumor cells and neovasculature dual targeting delivery for glioblastoma treatment, Biomaterials 35 (2014) 2374–2382.
[39] Z.Z. Yang, J.Q. Li, Z.Z. Wang, D.W. Dong, X.R. Qi, Tumor-targeting dual peptides-modified cationic liposomes for delivery of siRNA and docetaxel to gliomas, Biomaterials 35 (2014) 5226–5239.
[40] A. Ahmad, S. Sheikh, R. Taran, S.P. Srivastav, K. Prasad, S.J. Rajappa, V. Kumar, M. Gopichand, M. Paithankar, M. Sharma, R.C. Rane, I. Ahmad, Therapeutic efficacy of a novel nanosomal docetaxel lipid suspension compared with taxotere in locally advanced or metastatic breast cancer patients, Clin. Breast Cancer 14 (2014) 177–181.
[41] W.X. Qi, Z. Shen, F. Lin, Y.J. Sun, D.L. Min, L.N. Tang, A.N. He, Y. Yao, Paclitaxel-based versus docetaxel-based regimens in metastatic breast cancer: a systematic review and meta-analysis of randomized controlled trials, Curr. Med. Res. Opin. 29 (2013) 117–125.
[42] H. Joensuu, J. Gligorov, Adjuvant treatments for triple-negative breast cancers, Ann. Oncol. 23 (2012) vi40–vi45.
[43] M. Sanson, M. Napolitano, R. Yaya, F. Keime-Guibert, P. Broet, K. Hoang-Xuan, J.Y. Delattre, Second line chemotherapy with docetaxel in patients with recurrent malignant glioma: a phase II study, J. Neuro-Oncol. 50 (2000) 245–249.
[44] P. Forsyth, G. Cairncross, D. Stewart, M. Goodyear, N. Wainman, E. Eisenhauer, Phase II trial of docetaxel in patients with recurrent malignant glioma: a study of the National Cancer Institute of Canada Clinical Trials Group, Investig. New Drugs 14 (1996) 203–206.
[45] Taxotere® (docetaxel for injection), Product Monograph, Sanofi-Aventis Canada Inc., 2015 (http://products.sanofi.ca/en/taxotere.pdf).
[46] V.K. Venishetty, R. Komuravelli, M. Kuncha, R. Sistla, P.V. Diwan, Increased brain uptake of docetaxel and ketoconazole loaded folate-grafted solid lipid nanoparticles, Nanomedicine 9 (2013) 111–121.
[47] H. Gao, S. Zhang, S. Cao, Z. Yang, Z. Pang, X. Jiang, Angiopep-2 and activatable cell-penetrating peptide dual-functionalized nanoparticles for systemic glioma-targeting delivery, Mol. Pharm. 11 (2014) 2755–2763.
[48] H. Gao, S. Zhang, Z. Yang, S. Cao, X. Jiang, Z. Pang, In vitro and in vivo intracellular distribution and anti-glioblastoma effects of docetaxel-loaded nanoparticles functioned with IL-13 peptide, Int. J. Pharm. 466 (2014) 8–17.
[49] I. Puskas, A. Szemjonov, E. Fenyvesi, M. Malanga, L. Szente, Aspects of determining the molecular weight of cyclodextrin polymers and oligomers by static light scattering, Carbohydr. Polym. 94 (2013) 124–128.
[50] B. Bachmeier, A.G. Nerlich, C.M. Iancu, M. Cilli, E. Schleicher, R. Vene, R. Dell'Eva, M. Jochum, A. Albini, U. Pfeffer, The chemopreventive polyphenol curcumin prevents hematogenous breast cancer metastases in immunodeficient mice, Cell. Physiol. Biochem. 19 (2007) 137–152.
[51] M.J. Ernsting, W.L. Tang, N.W. MacCallum, S.D. Li, Preclinical pharmacokinetic, biodistribution, and anti-cancer efficacy studies of a docetaxel-carboxymethylcellulose nanoparticle in mouse models, Biomaterials 33 (2012) 1445–1454.
[52] T.K. Kim, I.S. Kim, H.H. Yoo, Determination of docetaxel in rat plasma and its application in the comparative pharmacokinetics of Taxotere and SID530, a novel docetaxel formulation with hydroxypropyl-beta-cyclodextrin, Biomed. Chromatogr. 27 (2013) 306–310.
[53] P. Prasad, A. Shuhendler, P. Cai, A.M. Rauth, X.Y. Wu, Doxorubicin and mitomycin C co-loaded polymer-lipid hybrid nanoparticles inhibit growth of sensitive and multidrug resistant human mammary tumor xenografts, Cancer Lett. 334 (2013) 263–273.
[54] J. Kreuter, D. Shamenkov, V. Petrov, P. Ramge, K. Cychutek, C. Koch-Brandt, R. Alyautdin, Apolipoprotein-mediated transport of nanoparticle-bound drugs across the blood-brain barrier, J. Drug Target. 10 (2002) 317–325.
[55] Y. Zhou, C. He, K. Chen, J. Ni, Y. Cai, X. Guo, X.Y. Wu, A new method for evaluating actual drug release kinetics of nanoparticles inside dialysis devices via numerical deconvolution, J. Control. Release 243 (2016) 11–20.
[56] B. Petri, A. Bootz, A. Khalansky, T. Hekmatara, R. Muller, R. Uhl, J. Kreuter, S. Gelperina, Chemotherapy of brain tumour using doxorubicin bound to surfactant-coated poly(butyl cyanoacrylate) nanoparticles: revisiting the role of surfactants, J. Control. Release 117 (2007) 51–58.
[57] J. Kreuter, T. Hekmatara, S. Dreis, T. Vogel, S. Gelperina, K. Langer, Covalent attachment of apolipoprotein A-I and apolipoprotein B-100 to albumin nanoparticles enables drug transport into the brain, J. Control. Release 118 (2007) 54–58.
[58] R.D. Zhang, I.J. Fidler, J.E. Price, Relative malignant potential of human breast carcinoma cell lines established from pleural effusions and a brain metastasis, Invasion Metastasis 11 (1991) 204–215.
[59] T. Yoneda, P.J. Williams, T. Hiraga, M. Niewolna, R. Nishimura, A bone-seeking clone exhibits different biological properties from the MDA-MB-231 parental human breast cancer cells and a brain-seeking clone in vivo and in vitro, J. Bone Miner. Res. 16 (2001) 1486–1495.
[60] J.E. Fardell, J. Zhang, R. De Souza, J. Vardy, I. Johnston, C. Allen, J. Henderson, M. Piquette-Miller, The impact of sustained and intermittent docetaxel chemotherapy regimens on cognition and neural morphology in healthy mice, Psychopharmacology 231 (2014) 841–852.
[61] A.A. van der Veldt, N.H. Hendrikse, E.F. Smit, M.P. Mooijer, A.Y. Rijnders, W.R. Gerritsen, J.J. van der Hoeven, A.D. Windhorst, A.A. Lammertsma, M. Lubberink, Biodistribution and radiation dosimetry of 11C-labelled docetaxel in cancer patients, Eur. J. Nucl. Med. Mol. Imaging 37 (2010) 1950–1958.
[62] M. Hart, S. Acott, Physical and chemical stability of Taxotere (docetaxel) one-vial (20 mg/mL) infusion solution following refrigerated storage, Ecancermedicalscience 4 (2010) 202.
[63] F.K. Engels, R.A.A. Mathot, J. Verweij, Alternative drug formulations of docetaxel: a review, Anti-Cancer Drugs 18 (2007) 95–103.
[64] D.Y. Joh, L. Sun, M. Stangl, A. Al Zaki, S. Murty, P.P. Santoiemma, J.J. Davis, B.C. Baumann, M. Alonso-Basanta, D. Bhang, G.D. Kao, A. Tsourkas, J.F. Dorsey, Selective targeting of brain tumors with gold nanoparticle-induced radiosensitization, PLoS One 8 (2013), e62425. .
[65] X. Wei, X. Chen, M. Ying, W. Lu, Brain tumor-targeted drug delivery strategies, Acta Pharm. Sin. B 4 (2014) 193–201.
[66] J.M. Gallo, S. Li, P. Guo, K. Reed, J. Ma, The effect of P-glycoprotein on paclitaxel brain and brain tumor distribution in mice, Cancer Res. 63 (2003) 5114–5117.
[67] M.E. Davis, Z. Chen, D.M. Shin, Nanoparticle therapeutics: an emerging treatment modality for cancer, Nat. Rev. Drug Discov. 7 (2008) 771–782.